

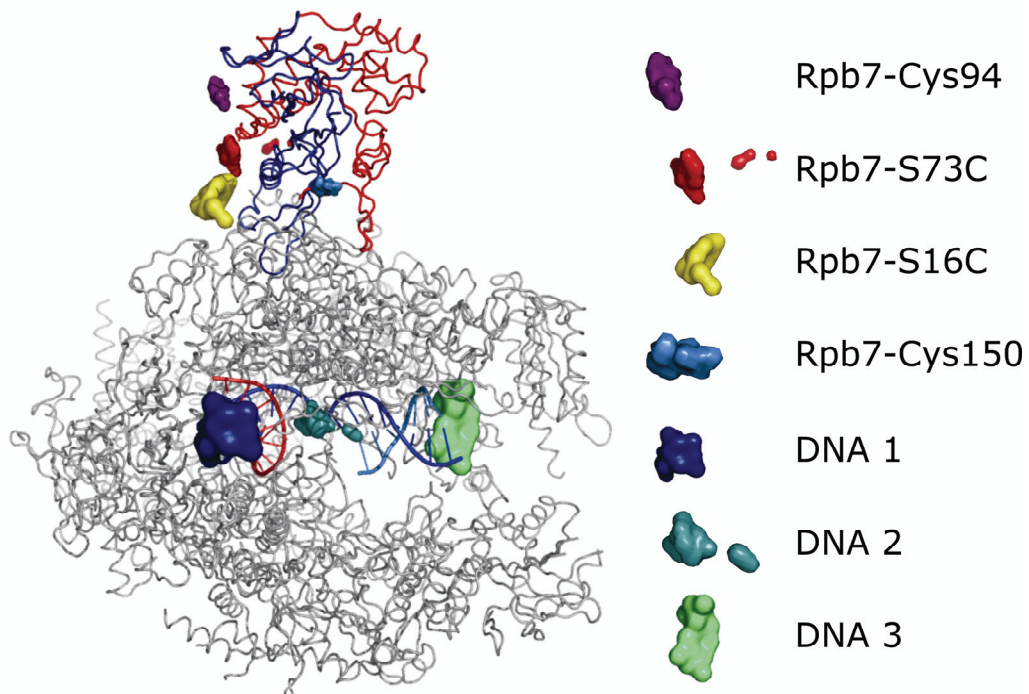
A nano-positioning system for macromolecular structural analysis

Adam Muschielok, Joanna Andrecka, Anass Jawhari, Florian Brückner, Patrick Cramer & Jens Michaelis

Supplementary figures and text:

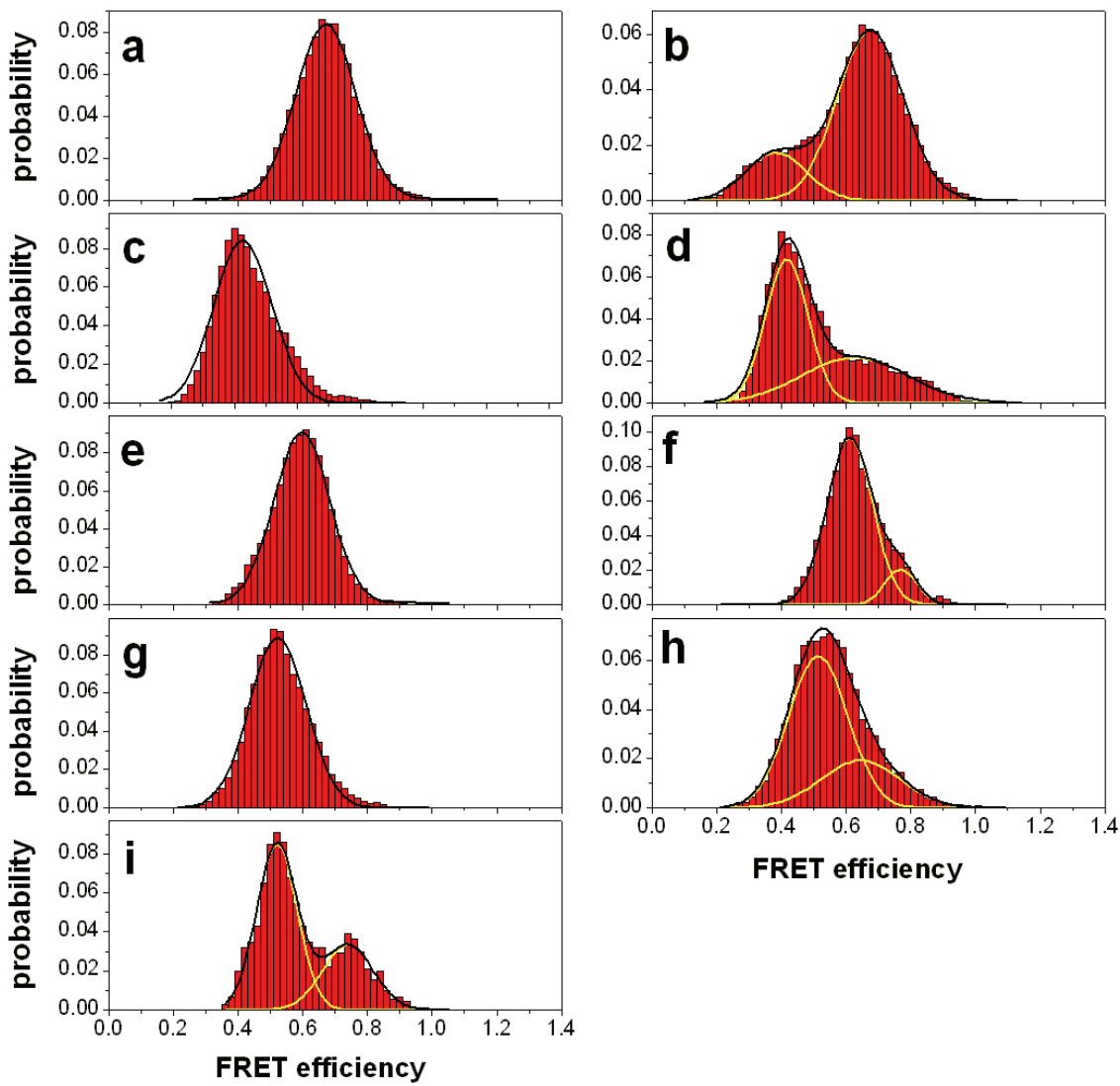
Supplementary Figure 1	Locations of the ‘satellite dye molecule’ positions
Supplementary Figure 2	FRET histograms of RNA 1 measurements
Supplementary Figure 3	FRET histograms of RNA 29 measurements
Supplementary Figure 4	DNA1 in presence of TFIIB
Supplementary Figure 5	Pol II pull down experiments
Supplementary Figure 6	Radial profiles of fuzzy spheres of RNA 1
Supplementary Figure 7	Radial profiles of fuzzy spheres of RNA 29
Supplementary Figure 8	Förster radius priors
Supplementary Table 1	Fluorescence anisotropies
Supplementary Methods	

Supplementary Figure 1



Supplementary Figure 1: Locations of the ‘satellite dye molecule’ positions. Top view of the elongation complex with Pol II core (grey), Rpb4 (blue), Rpb7 (red), template DNA strand (blue), non-template DNA strand (cyan) and RNA product (red). The location of the satellite dye molecule positions is indicated by the small icons.

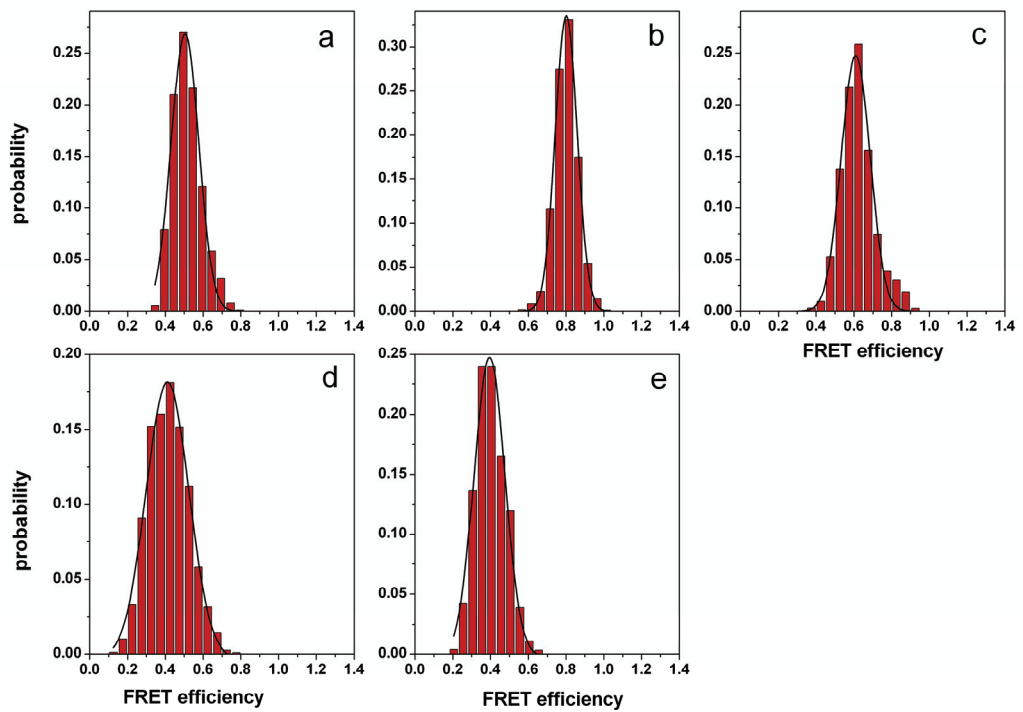
Supplementary Figure 2



Supplementary Figure 2: FRET histograms of RNA 29 measurements.

Histograms of the measured FRET efficiency obtained in the absence (**a,c,e,g,i**) and presence (**b,d,f,h**) of TFIIB for the labelling sites DNA1 (**a,b**), DNA2 (**c,d**), Rpb7-Cys150 (**e,f**), Rpb7-Cys94 (**g,h**) and Rpb7-S73C (**i**). Either single or double Gaussians (black line, in the latter case the individual Gaussians are shown in yellow) were fitted to each histogram.

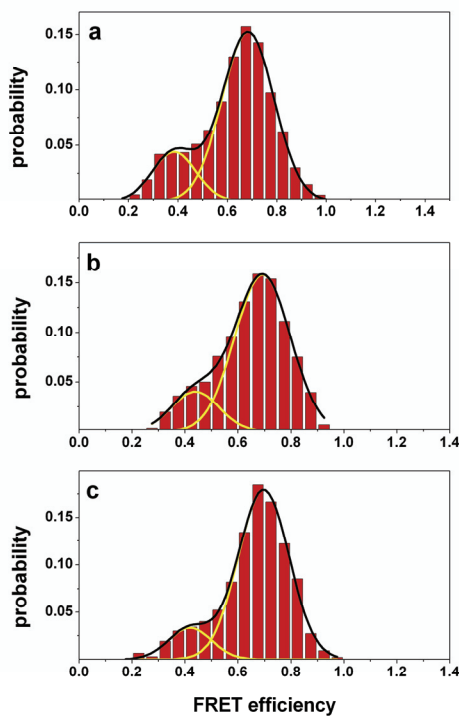
Supplementary Figure 3



Supplementary Figure 3: FRET histograms of RNA 1 measurements.

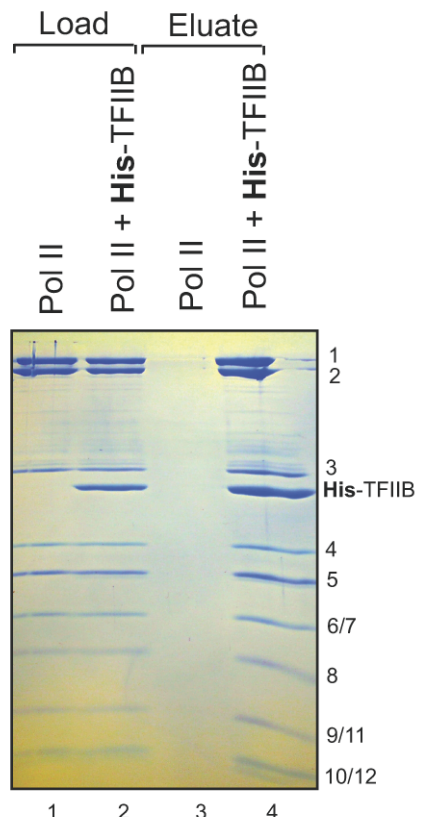
Shown are the histograms of the measurements with the donor attached to the RNA 3' end and the acceptor attached to DNA 1 (**a**), DNA 2 (**b**), DNA 3 (**c**), Rpb7-Cys150 (**d**) and Rpb7-S16C (**e**). As a donor dye Alexa 555 (**a-c, e**) or TMR (**d**) and as an acceptor dye Alexa 647 was used. Gaussian fits to the histograms are shown by black lines.

Supplementary Figure 4



Supplementary Figure 4: FRET histograms for the RNA 29 in presence of TFIIB. Shown are the histograms for complexes labelled with the SDM at DNA 1 and ADM at RNA 29 position after wild-type TFIIB was incubated in the chamber (**a**) (the same as histogram in Supplementary Fig. 2b), TFIIB B-finger deletion mutant incubated in the chamber (**b**) and pre-incubated (**c**).

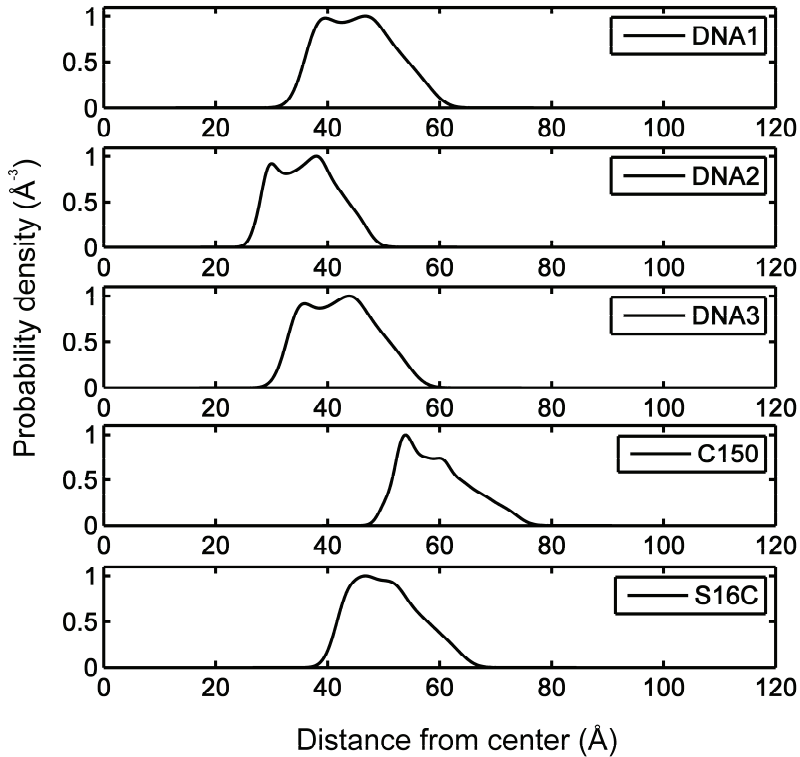
Supplementary Figure 5



Supplementary Figure 5: Pull down experiments. In order to investigate the interaction between TFIIB and Pol II, a Pol II pull down assay was carried out. In this assay a His-tagged version of highly purified TFIIB, as well as pure untagged Pol II stored in assembly buffer were used.

Typically 50 micrograms of Pol II was first incubated with pre-annealed DNA/RNA scaffold (1.5x excess) at 20°C for 10 minutes and then incubated with His-TFIIB (1.5x excess) for 60 minutes in presence of 50µl of Ni-NTA resin. After extensive washing using assembly buffer containing 0.1% Np40, the protein was eluted by addition of the same buffer containing 100 mM imidazol. As negative control, Pol II was loaded to Ni-NTA resin, washed and eluted. The load and eluate were analysed by SDS-PAGE and Coomassie staining. The gel shows a typical result of the experiment, demonstrating that we observed binding to the resin only in the presence of His-TFIIB.

Supplementary Figure 6

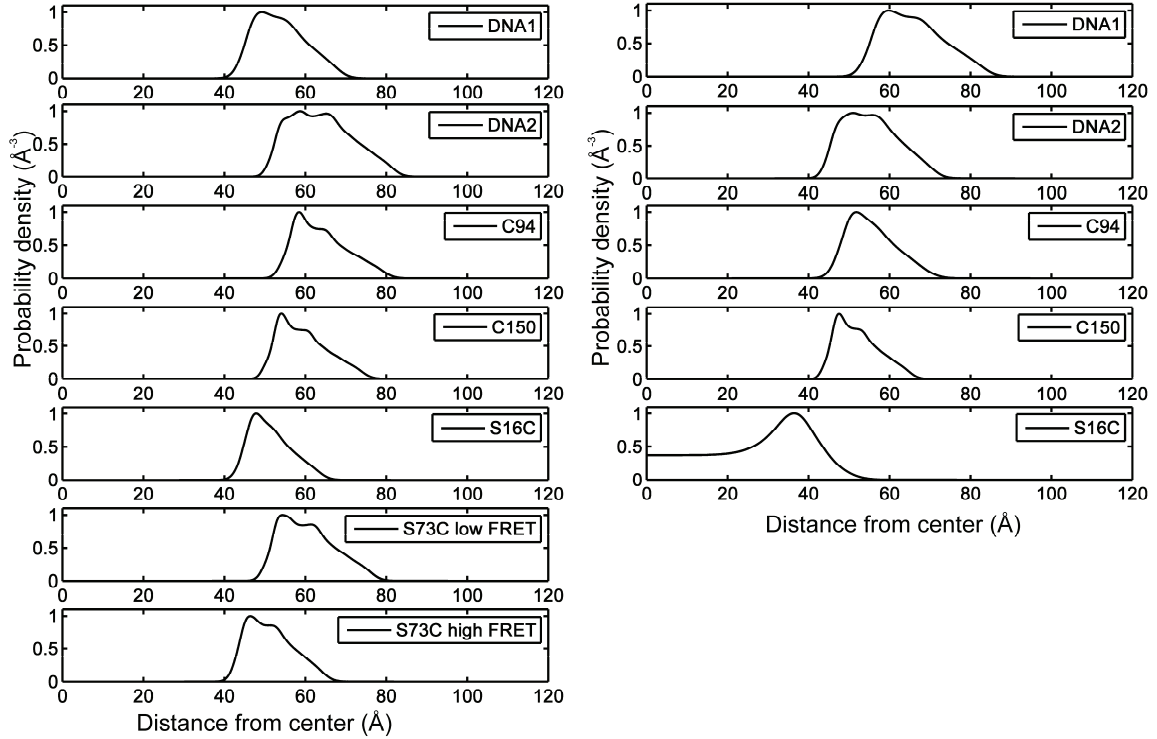


Supplementary Figure 6: Radial profiles of fuzzy spheres of RNA 1

The radial profiles $F_{ij}(d_{ij})$ of the fuzzy spheres $K_{ij}(\mathbf{x})$ for the satellite dye molecules are displayed. The profiles are normalised to maximum = 1 and plotted over the distance in Å. Note that since the SDM priors are not spherically symmetric in this case, the contribution of the measured ADM-SDM pair i consists of the superposition of several fuzzy spheres,

$$K_i(\mathbf{x}) = \sum_i w_{ij} K_{ij}(\mathbf{x}).$$

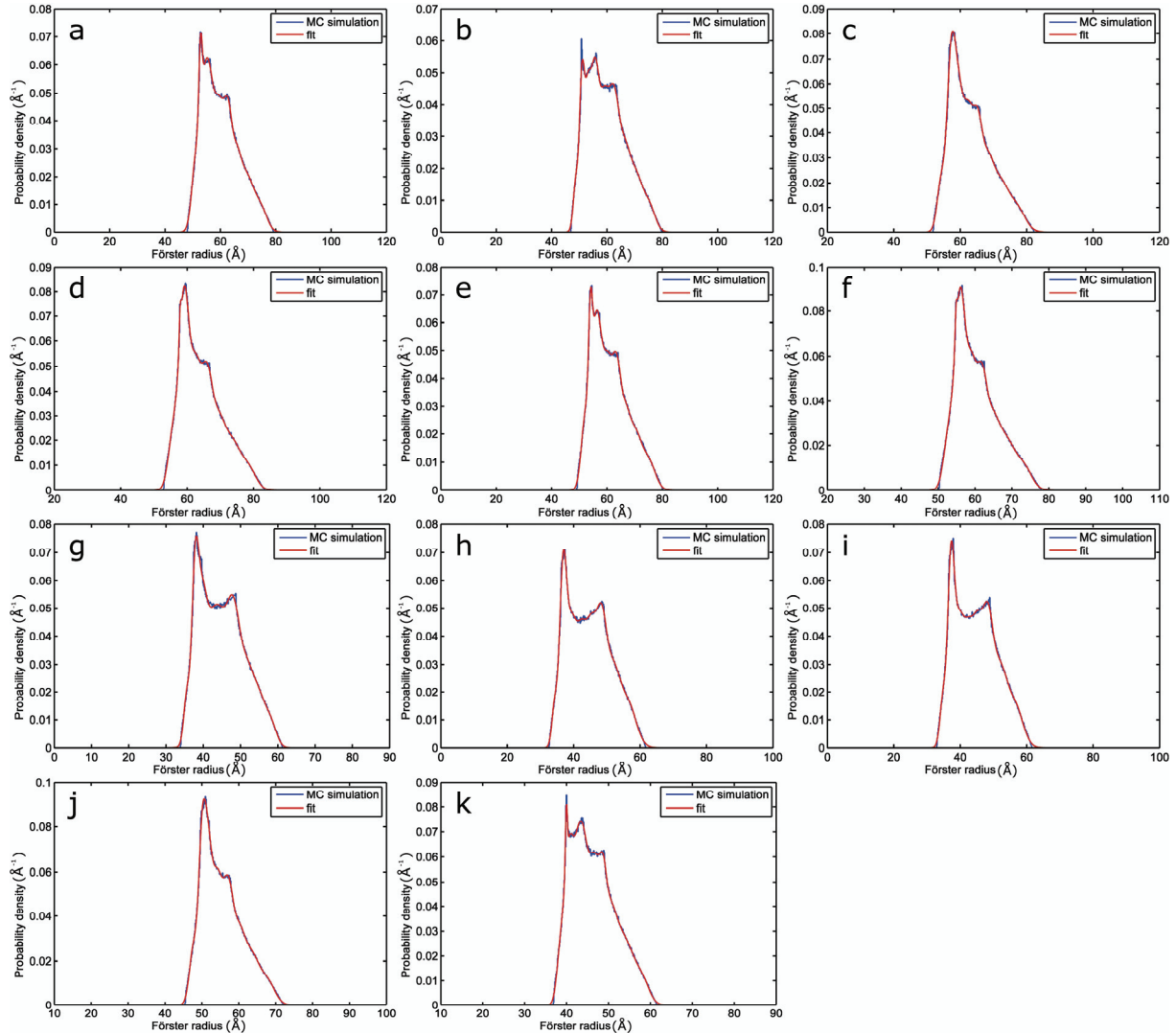
Supplementary Figure 7



Supplementary Figure 7: Radial profiles of fuzzy spheres of RNA 29

The radial profiles $F_{ij}(d_{ij})$ of the fuzzy spheres $K_{ij}(\mathbf{x})$ for the satellite dye molecules are displayed. The profiles are normalised to maximum = 1 and plotted over the distance in Å. Note that since the SDM priors are not spherically symmetric in this case, the contribution of the measured ADM-SDM pair i consists of the superposition of several fuzzy spheres, $K_i(\mathbf{x}) = \sum_i w_{ij} K_{ij}(\mathbf{x})$.

Supplementary Figure 8



Supplementary Figure 8: Förster radius priors. The probability densities were obtained by Monte-Carlo simulations of Förster radii given an isotropic distribution of the average dye molecule orientation. (a) DNA 1(Alexa647)-RNA 29(TMR), (b) DNA 2(Alexa647)-RNA 29(TMR), (c) Rpb7-Cys150(Alexa647)-RNA 29(TMR), (d) Rpb7-Cys94(Alexa647)-RNA 29(TMR), (e) Rpb7-S73C(Alexa647)-RNA 29(TMR), (f) Rpb7-S16C(Alexa647)-RNA 29(TMR), (g) DNA 1(Alexa647)-RNA 1(Alexa555), (h) DNA 2(Alexa647)-RNA 1(Alexa555), (i) DNA 3(Alexa647)-RNA 1(Alexa555), (j) Rpb7-Cys150(Alexa647)-RNA 1(TMR), (k) Rpb7-S16C(Alexa647)-RNA 1(Alexa555) (TMR: tetramethylrhodamine)

Supplementary Table 1: Fluorescence anisotropies

Labelling site	Dye	Fluorescence anisotropy (\pm SD)
RNA 1	<i>TMR</i> ¹	0.210 \pm 0.007
RNA 1	<i>Alexa 555</i>	0.310 \pm 0.011
RNA 29	<i>TMR</i> ¹	0.210 \pm 0.008
RNA 29 (TFIIB)	<i>TMR</i> ¹	0.210 \pm 0.009
DNA 1	<i>Alexa 647</i>	0.30 \pm 0.01
DNA 2	<i>Alexa 647</i>	0.320 \pm 0.016
DNA 3	<i>Alexa 647</i>	0.310 \pm 0.004
Rpb7-Cys150	<i>Alexa 647</i>	0.230 \pm 0.016
Rpb7-Cys94	<i>Alexa 647</i>	0.220 \pm 0.004
Rpb7-S73C	<i>Alexa 647</i>	0.270 \pm 0.008
Rpb7-S16C	<i>Alexa 647</i>	0.200 \pm 0.006

¹⁾ TMR: tetramethylrhodamine

SUPPLEMENTARY METHODS

1. PRIOR

As stated in the main text, the prior can be factorised into the independent contributions from each of the model parameters

$$p(\mathbf{x}, \{\mathbf{s}_i\}, \{R_i\} | I) = p(\mathbf{x}|I) \prod_i [p(\mathbf{s}_i|I)p(R_i|I)], \quad (1)$$

where $\{\mathbf{s}_i\} = (\mathbf{s}_1, \dots, \mathbf{s}_N)$ are the satellite dye molecule positions, $\{R_i\} = (R_1, \dots, R_N)$ are the Förster radii, and \mathbf{x} is the antenna dye molecule position. The contributions of the antenna dye molecule (ADM) prior, $p(\mathbf{x}|I)$, the satellite dye molecules (SDMs), $p(\mathbf{s}_i|I)$, and the Förster radii, $p(R_i|I)$, are discussed in the following.

1.1. Calculation of volumes accessible to the dye molecules. In our analysis we exclude antenna and satellite dye molecule positions that cause a steric clash with the macromolecular complex. A clash is defined by Van der Waals contact of either dye or linker with the macromolecular complex. In order to calculate the volumes that are accessible to the dyes we approximate the dye with a sphere with diameter D_{dye} that is attached to the macromolecule with a flexible linker that has the thickness D_{linker} and the length L_{linker} . In our case, we used $D_{\text{dye}} = 7\text{\AA}$ for all dyes, $L_{\text{linker}} = 13\text{\AA}$ for satellite dyes attached to DNA 1, DNA 2 or DNA 3, $L_{\text{linker}} = 7\text{\AA}$ for the remaining satellite dyes, $L_{\text{linker}} = 7\text{\AA}$ for the antenna dye on RNA 1, and $L_{\text{linker}} = 92\text{\AA}$ for the antenna dye on RNA 29. The linker diameter was $D_{\text{linker}} = 4.5\text{\AA}$ for all satellite dyes and the antenna dye on RNA 1, and $D_{\text{linker}} = 9.4\text{\AA}$ for the antenna dye on RNA 29. The structure of the macromolecular complex was taken from the Protein Data Bank (PDB format). The labelling sites were C6 in the case of DNA 1, DNA 2 and DNA 3, O3 in the case of RNA 1 on the respective nucleic acids. The labelling sites on the protein were the sulfur atoms of the respective cysteins (we used the coordinates of the oxygen atom in the serine residues that were mutated to cysteins).

1.2. Antenna dye molecule position prior. We assume the antenna dye molecule position prior $p(\mathbf{x}|I)$ to be constant inside V_A , the volume that is accessible to the antenna dye, and 0 outside of V_A .

$$p(\mathbf{x}|I) = \begin{cases} C^{st} & \mathbf{x} \in V_A \\ 0 & \text{else} \end{cases} \quad (2)$$

1.3. Satellite dye molecule position prior. We express the prior probability distribution for each satellite dye molecule position s_i as a weighted sum of isotropic three-dimensional Gaussians with center positions $\langle \mathbf{s} \rangle_{ij}$, standard deviations Δs_{ij} and weights w_{ij}

$$\begin{aligned} p(\mathbf{s}_i | I) &= \sum_j w_{ij} \left(\sqrt{2\pi} \Delta s_{ij} \right)^{-3} \exp \left(-\frac{\left| \mathbf{s}_i - \langle \mathbf{s} \rangle_{ij} \right|^2}{2 (\Delta s_{ij})^2} \right) \\ &= \sum_j w_{ij} S_{ij}(\mathbf{s}_i), \end{aligned} \quad (3)$$

where we have abbreviated each Gaussian by $S_{ij}(\mathbf{s}_i)$. The weights for each satellite dye position sum up to 1 ($\sum_j w_{ij} = 1$).

We choose the centers $\langle \mathbf{s} \rangle_{ij}$, widths Δs_{ij} and weights w_{ij} such that the prior approximately describes the volume V_{S_i} which is accessible to the satellite dye,

$$p(\mathbf{s}_i|I) \approx \begin{cases} C^{st} & \mathbf{s}_i \in V_{S_i} \\ 0 & \text{else} \end{cases} \quad (4)$$

We used 15 Gaussians to model each satellite dye position. This was a good approximation of the accessible volumes and yielded a reasonable calculation time in the final analysis.

1.4. Monte-Carlo simulations of Förster radii probability densities. For the calculation of the prior $p(R_i|I)$ for each Förster radius R_i we assume that in each FRET pair the orientation of the ADM and SDM transition dipole moments is fluctuating around a preferred and fixed orientation. We also assume that these fluctuations are fast compared to the fluorescence lifetimes and that they result in an approximately axially symmetric angular distribution. With these assumptions we can calculate the Förster radius R_i [1],

$$R_i = R_i^{\text{iso}} \sqrt[6]{\frac{3}{2} \langle \kappa^2 \rangle}, \quad (5)$$

where R_i^{iso} is the isotropic Förster radius as determined previously [2] and $\langle \kappa^2 \rangle$ is the dynamically averaged orientation factor. We calculate the latter using eq. 21 and 22 in [1]:

$$\begin{aligned} \langle \kappa^2 \rangle = & \kappa^{x2} \langle d_{\text{ADM}}^x \rangle \langle d_{\text{SDM}}^x \rangle + \frac{1}{3} (1 - \langle d_{\text{ADM}}^x \rangle) + \frac{1}{3} (1 - \langle d_{\text{SDM}}^x \rangle) \\ & + \cos^2 \Theta_{\text{ADM}} \langle d_{\text{ADM}}^x \rangle (1 - \langle d_{\text{SDM}}^x \rangle) + \cos^2 \Theta_{\text{SDM}} \langle d_{\text{SDM}}^x \rangle (1 - \langle d_{\text{ADM}}^x \rangle), \end{aligned} \quad (6)$$

in which

$$\kappa^{x2} = (\sin \Theta_{\text{ADM}} \sin \Theta_{\text{SDM}} \cos \Phi - 2 \cos \Theta_{\text{ADM}} \cos \Theta_{\text{SDM}})^2 \quad (7)$$

is the axial orientation factor defined for the preferred orientation, while $\langle d_{\text{ADM}}^x \rangle$ and $\langle d_{\text{SDM}}^x \rangle$ are the average depolarizations which we obtain from the measured bulk anisotropies r_{ADM} and r_{SDM} of ADM and SDM, respectively (eq. 33 in [1]):

$$\langle d_{\text{ADM/SDM}}^x \rangle = \begin{cases} \sqrt{r_{\text{ADM/SDM}}/0.4} & r_{\text{ADM/SDM}} > 0.1 \\ \pm \sqrt{r_{\text{ADM/SDM}}/0.4} & r_{\text{ADM/SDM}} \leq 0.1. \end{cases} \quad (8)$$

The mean orientation factor $\langle \kappa^2 \rangle$ depends on the relative preferred orientation of ADM and SDM, which is characterized by three angles: the angles between the preferred orientation of ADM and SDM to the line connecting both dyes, Θ_{ADM} and Θ_{SDM} , respectively, and the angle Φ between the two planes defined by each of the preferred orientations of both dyes and the connecting line. Since we do not know the preferred orientations, we give equal probabilities to all orientations and calculate random samples

$$\Theta_{\text{ADM}} = \arccos(\text{rand}(0, 1)) \quad (9)$$

$$\Theta_{\text{SDM}} = \arccos(\text{rand}(0, 1)) \quad (10)$$

$$\Phi = 2\pi \text{rand}(0, 1), \quad (11)$$

where $\text{rand}(0, 1)$ denotes (pseudo-)random numbers between 0 and 1. We insert the random preferred orientations into eqs. 5 - 8 in order to simulate possible Förster radii. From normalized histograms of the simulated Förster radii we obtain an analytic approximation for the Förster radius priors as discussed now.

1.5. Förster radius. We assign the prior probability distribution for each Förster radius R_i to be a linear combination of kernels $Q_{ik}(R_i)$

$$p(R_i|I) = \sum_k v_{ik} Q_{ik}(R_i), \quad (12)$$

where each kernel has image-charge-like shape

$$Q_{ik}(R_i) = \left[\sqrt{2\pi} \Delta \tilde{R}_{ik} \operatorname{erf} \left(\frac{\tilde{R}_{ik}}{\sqrt{2} \Delta \tilde{R}_{ik}} \right) \right]^{-1} \left\{ \exp \left[-\frac{(R_i - \tilde{R}_{ik})^2}{2(\Delta \tilde{R}_{ik})^2} \right] - \exp \left[-\frac{(R_i + \tilde{R}_{ik})^2}{2(\Delta \tilde{R}_{ik})^2} \right] \right\}. \quad (13)$$

For each Förster radius R_i the weights v_{ik} again sum up to 1 ($\sum_k v_{ik} = 1$). We choose the parameters \tilde{R}_{ik} , $\Delta \tilde{R}_{ik}$ and v_{ik} such that the prior approximates the simulated distribution of possible Förster radii.

2. LIKELIHOOD

As stated in the main text we can assign the likelihood to be the product of uncorrelated Gaussians

$$\begin{aligned} p(\{E_i\}|\boldsymbol{x}, \{\boldsymbol{s}_i\}, \{R_i\}, I) &= \prod_i p(E_i|\boldsymbol{x}, \boldsymbol{s}_i, R_i, I) \\ &= \prod_i \frac{\exp \left\{ -[\mathcal{E}_i(\boldsymbol{x}, \boldsymbol{s}_i, R_i) - E_i]^2 / [2(\Delta E_i)^2] \right\}}{\Delta E_i \sqrt{2\pi}} \\ &= \prod_i L_i(|\boldsymbol{x} - \boldsymbol{s}_i|/R_i), \end{aligned} \quad (14)$$

where $\mathcal{E}_i(\boldsymbol{x}, \boldsymbol{s}_i, R_i)$ is the FRET efficiency expected for a given Förster radius, antenna dye position and satellite dye position,

$$\mathcal{E}_i(\boldsymbol{x}, \boldsymbol{s}_i, R_i) = \frac{1}{1 + (|\boldsymbol{x} - \boldsymbol{s}_i|/R_i)^6}, \quad (15)$$

and we denoted the contribution of the i^{th} measurement to the likelihood by $L_i(|\boldsymbol{x} - \boldsymbol{s}_i|/R_i)$. The measured FRET efficiencies, E_i , can be obtained from least-squares fits to the FRET histograms. The respective uncertainties, ΔE_i , are calculated by properly propagated errors $\Delta E_{i,\text{fit}}$ of the fit and the systematic errors $\Delta E_{i,\text{sys}}$

$$\Delta E_i = \sqrt{(\Delta E_{i,\text{sys}})^2 + (\Delta E_{i,\text{fit}})^2}. \quad (16)$$

3. POSTERIOR

Within the approximations used for the likelihood and prior, the posterior probability density factorizes into

$$p(\boldsymbol{x}, \{\boldsymbol{s}_i\}, \{R_i\} | \{E_i\}, I) \propto p(\boldsymbol{x}|I) \prod_i p(E_i|\boldsymbol{x}, \boldsymbol{s}_i, R_i, I) p(\boldsymbol{s}_i|I) p(R_i|I). \quad (17)$$

3.1. Calculating the antenna dye position posterior. In the present approach we are only interested in the information about the position of the ADM and do not in information about SDM positions and Förster radii. Hence, we calculated the antenna dye position posterior, i.e. the probability density $p(\mathbf{x}|\{E_i\}, I)$ by integration of the posterior over the satellite dye positions \mathbf{s}_i and the Förster radii R_i :

$$\begin{aligned} p(\mathbf{x}|\{E_i\}, I) &\propto \iint p(\mathbf{x}, \{\mathbf{s}_i\}, \{R_i\}|\{E_i\}, I) d\{\mathbf{s}_i\} d\{R_i\} \\ &= p(\mathbf{x}|I) \prod_i \iint L_i(|\mathbf{x} - \mathbf{s}_i|/R_i) p(\mathbf{s}_i|I) p(R_i|I) d\mathbf{s}_i dR_i \\ &= p(\mathbf{x}|I) \prod_i \sum_j \iint L_i(|\mathbf{x} - \mathbf{s}_i|/R_i) w_{ij} S_{ij}(\mathbf{s}_i) p(R_i|I) d\mathbf{s}_i dR_i \\ &= p(\mathbf{x}|I) \prod_i \sum_j w_{ij} K_{ij}(\mathbf{x}). \end{aligned} \quad (18)$$

Note, that for a fixed antenna dye position \mathbf{x} each combination of the remaining parameters $\{\mathbf{s}_i\}$ and $\{R_i\}$ contributes to $p(\mathbf{x}|\{E_i\}, I)$ with its probability, $p(\mathbf{x}, \{\mathbf{s}_i\}, \{R_i\}|\{E_i\}, I)$.

We want to discuss the 4-dimensional (3 dimensions for \mathbf{s}_i and 1 for R_i) integrals for $K_{ij}(\mathbf{x})$ from the equation above in detail. We used Maple to integrate over three out of 4 dimensions analytically: we chose spherical coordinates in \mathbf{s}_i around \mathbf{x} , $(s_i^x - x^x, s_i^y - x^y, s_i^z - x^z) \rightarrow (s_i, \theta_i, \phi_i)$, and integrated over the angular variables first to obtain the expression:

$$K_{ij}(\mathbf{x}) = \sum_k v_{ik} \int_0^\infty \int_0^\infty L_i(s_i/R_i) \frac{s_i}{\sqrt{2\pi} \Delta s_{ij} d_{ij}} \left[\exp\left(-\frac{(s_i - d_{ij})^2}{2(\Delta s_{ij})^2}\right) - \exp\left(-\frac{(s_i + d_{ij})^2}{2(\Delta s_{ij})^2}\right) \right] Q_{ik}(R_i) dR_i ds_i \quad (19)$$

where $d_{ij} = |\mathbf{x} - \langle \mathbf{s} \rangle_{ij}|$. Since $K_{ij}(\mathbf{x})$ depends not directly on \mathbf{x} but on the distance d_{ij} only, it possesses spherical symmetry around the point $\langle \mathbf{s} \rangle_{ij}$. Consequently, we calculate $K_{ij}(\mathbf{x})$ by evaluating its radial profile $F_{ij}(d_{ij})$

$$K_{ij}(\mathbf{x}) = F_{ij}(d_{ij}) = \sum_k v_{ik} F_{ijk}(d_{ij}), \quad (20)$$

where $F_{ijk}(d_{ij})$ is the contribution of the k^{th} kernel in the Förster radius prior to the radial profile $F_{ij}(d_{ij})$. In order to calculate $F_{ijk}(d_{ij})$ we use equation 12, transform the integration coordinates $(s_i, R_i) \rightarrow (s_i, r_i) = (s_i, R_i/s_i)$, and integrate over s_i . Doing this we arrive at the lengthy expression

$$\begin{aligned} F_{ijk}(d_{ij}) &= \left[\sqrt{2\pi} d_{ij} \operatorname{erf}\left(\tilde{R}_{ik}/\sqrt{2}\Delta\tilde{R}_{ik}\right) \right]^{-1} \\ &\int_0^\infty \frac{L_i(1/r_i)}{\left[\left(\Delta\tilde{R}_{ik}\right)^2 + r_i^2 (\Delta s_{ij})^2\right]^{5/2}} \left\{ \left[\left(\tilde{R}_{ik}^2 + (\Delta\tilde{R}_{ik})^2\right) (\Delta s_{ij})^4 r_i^2 + \right. \right. \\ &\left. \left. \left(d_{ij}^2 + (\Delta s_{ij})^2\right) (\Delta\tilde{R}_{ik})^4 \right] X_- + 2 \left[d_{ij} \left(\Delta\tilde{R}_{ik}\right)^2 \tilde{R}_{ik} r_i (\Delta s_{ij})^2 \right] X_+ \right\} dr_i \end{aligned} \quad (21)$$

where

$$X_\pm = \exp \left[-\frac{\frac{1}{2}(d_{ij}r_i - \tilde{R}_{ik})^2}{(\Delta\tilde{R}_{ik})^2 + r_i^2(\Delta s_{ij})^2} \right] \pm \exp \left[-\frac{\frac{1}{2}(d_{ij}r_i + \tilde{R}_{ik})^2}{(\Delta\tilde{R}_{ik})^2 + r_i^2(\Delta s_{ij})^2} \right] \quad (22)$$

We sample the radial profiles $F_{ijk}(d_{ij})$ in several hundred support points on the d_{ij} -axis by solving the integral in equation 21 numerically. For integration we use adaptive quadrature that is implemented in the MATLAB function `quadgk` [3]. In the next step we calculate the radial profile $F_{ij}(d_{ij})$ of the fuzzy sphere (eq. 20), and linearly interpolate it to calculate $K_{ij}(\mathbf{x})$ on a cubic lattice (1 Å spacing).

Finally, we add the fuzzy spheres that contribute to the same FRET measurement (i.e. $K_{ij}(\mathbf{x})$ for a fixed i) and multiply all resulting sums and the antenna dye position prior (eq. 18). In this way we calculate $p(\mathbf{x}|\{E_i\}, I)$, the antenna dye posterior, which is unnormalized yet. The normalization constant Z which is called *evidence* in the Bayesian framework is calculated by approximately solving the integral

$$Z = \int p(\mathbf{x}|\{E_i\}, I) d\mathbf{x}. \quad (23)$$

We use trapezoidal integration of the sampled density implemented in the MATLAB function `trapz` in order to calculate Z , and normalized $p(\mathbf{x}|\{E_i\}, I)$.

3.2. Summarizing the antenna dye position posterior in a few numbers. Having calculated the antenna dye posterior density (sampled on a cubic lattice) we determine the coordinates of the lattice point with the highest probability density. We also calculate the average antenna dye position $\langle \mathbf{x} \rangle$ and the covariance matrix $\text{Cov}(\mathbf{x})$:

$$\langle \mathbf{x} \rangle = \int \mathbf{x} p(\mathbf{x}|\{E_i\}, I) d\mathbf{x} \quad (24)$$

$$\text{Cov}(\mathbf{x}) = \int (\mathbf{x} - \langle \mathbf{x} \rangle)(\mathbf{x} - \langle \mathbf{x} \rangle)^T p(\mathbf{x}|\{E_i\}, I) d\mathbf{x} \quad (25)$$

These integrals are computed approximately by trapezoidal integration. In order to compute the error of the triangulation we diagonalise $\text{Cov}(\mathbf{x})$. If the posterior is unimodal, the error in the three principal directions is the square root of the diagonalised covariance matrix elements.

3.3. Displaying credibility volumes. We iteratively determine the probability density levels p_m that enclose a volume with the given credibility level P_m ,

$$P_m = \int_{p(\mathbf{x}|\{E_i\}, I) \geq p_m} p(\mathbf{x}|\{E_i\}, I) d\mathbf{x}. \quad (26)$$

The value of p_m for a specific credibility level P_m will vary for different ADM posteriors. Since we want to display the respective credibility volumes in an external program without knowing p_m explicitly, we transform $p(\mathbf{x}|\{E_i\}, I)$ with a monotonic function $f(p)$ that sets the previously obtained density levels p_m on the defined levels c_m , $f(p_m) = c_m$,

$$c(\mathbf{x}) = f(p(\mathbf{x}|\{E_i\}, I)). \quad (27)$$

In this way, the credibility level P_m is related to the level c_m , such that we can display surfaces of the corresponding credibility volumes by plotting isosurfaces to the value c_m . The function $c(\mathbf{x})$ is saved in XPLOR density format and can be loaded with common molecular viewing software.

Table of saved credibility levels

P_m	1	0.9545	0.68269	0.38292	0.1	0.05	0.01	0
c_m	0	0.5	1	2	3	4	5	6

REFERENCES

- [1] R.E. Dale, J. Eisinger, and W.E. Blumberg. The orientational freedom of molecular probes. the orientation factor in intramolecular energy transfer. *Biophysical Journal*, 26:161–193, 1979.
- [2] J. Andrecka, R. Lewis, F. Brückner, E. Lehmann, P. Cramer, and J. Michaelis. Single-molecule tracking of mrna exiting from rna polymerase ii. *Proc Natl Acad Sci U S A*, 105(1):135–140, Jan 2008.
- [3] L.F. Shampine. Vectorized adaptive quadrature in matlab. *Journal of Computational and Applied Mathematics*, 211:131–140, 2008.